



## Discrimination of Arctic multi-year ice from first-year ice using SCATSAT-1 data

Khoisnam Nanaoba Singh<sup>a</sup>, Urikhibam Somas Singh<sup>a</sup> & Rajkumar Kamaljit Singh<sup>\*</sup>

<sup>a</sup>Department of Physics, National Institute of Technology Manipur, Langol, Imphal, Manipur 795 004, India

<sup>b</sup>Department of Physics, Manipur Technical University, Takyelpat, Imphal, Manipur 795 004, India

*Received: 10 January 2020; accepted: 2 September 2020*

The distinctive dielectric properties of multi-year ice that make it stand out from the first-year ice has been exploited in this study to discriminate the Arctic multi-year ice from the first-year ice. We have used the backscattering coefficient, the brightness temperature and the gamma-naught data from the ISRO's miniature satellite SCATSAT-1 for this study. Principal component analysis in conjunction with the ISODATA unsupervised classification technique has been used to achieve the goal of this study. The classification results so obtained have been compared with a well-established sea ice type data product from the EUMETSAT's Ocean & Sea Ice Satellite Application Facility. Moreover, we have employed a change detection technique to ascertain the changes in the Arctic multi-year ice for the SCATSAT-1 period 2016 through 2018 (autumn and spring changes).

**Keywords:** Multi-year ice, SCATSAT-1, Principal component analysis, ISODATA classification

### 1 Introduction

The importance of sea ice in the global climate system can be understood from its constant interaction with the ocean that lies underneath it and the atmosphere just above it. Based on the stage of development, sea ice can be classified into a variety of ice types. However, a broad classification can be used which categorizes sea ice as a) the seasonal/first year ice-FYI (which reforms each winter and disappears by the end of the melting season with thickness of about 2 m), and b) the perennial/multi-year ice-MYI (which survives at least one summer melt and thickness in the range between 2 to 6 m)<sup>1</sup>. Owing to the differences in the geographical settings of the Arctic and the Antarctic, there is more MYI in the Arctic as compared to that in the Antarctic<sup>2</sup>. Moreover, in the Antarctic, the persistence of MYI is owing to the circulating current in the Weddell Sea, on the eastern side of the Antarctic Peninsula<sup>3</sup>. Thus, in the Arctic, the thicker MYI with higher albedo is of particular interest than the thinner FYI. Arctic MYI provides more stability to the ice cover. However, it poses more danger to sea vessels than FY ice<sup>4</sup>.

The changing of an Arctic Ocean mostly covered by MYI to one with mostly FYI due to melting of large areas with MYI will have major impacts on the Arctic climate system and marine activities. The

thinner FYI leads to warmer Arctic environment<sup>1</sup>. In the study of the Arctic MYI for the winters of 1979–2011, it was found that there was a rapid decline of the MYI, with a record low in 2008. But it subsequently got recovered in 2009–2011<sup>5</sup>. It was opined that such declines in the Arctic MYI would mean a reduction in the average ice thickness and an even more vulnerable perennial ice cover. Similar decline in the Arctic MYI was also found by using a five-year (from 2003 to 2008) altimeter, submarine cruise and moorings data<sup>6</sup>. Their study concluded that, in the 4 years following 2005, there was a net loss in MYI volume of 6300 km<sup>3</sup> (about 42% decreases). In a recent study<sup>7</sup>, a large decline in the MYI over major portions of the Arctic Ocean was observed, the highest coverage in 2002 (in excess of 4×10<sup>6</sup> km<sup>2</sup>) to less than 2×10<sup>6</sup> km<sup>2</sup> in 2017 (more than 50% loss).

Classification of sea ice types has been carried out using either active sensors<sup>4</sup> or passive sensors<sup>8</sup> or a combination of both<sup>9</sup>. It was opined that for sea ice classification into FYI and MYI, microwave backscatter produces more temporally stable results than microwave brightness temperature<sup>4,10</sup>. But since, both the techniques have been successfully employed by various researchers, we, in this study, combine both the microwave backscatter as well as the brightness temperature to achieve the common goal of FYI/MYI classification using the data from ISRO's SCATSAT-1.

\*Corresponding author (E-mail: kamaljit.rajkumar@gmail.com)

The work here is a follow-up of an earlier publication<sup>11</sup>. The manuscript is structured as follows. A brief discussion on the data used in this study is given in the next section (Satellite data), while the discussion on the classification technique and methodology employed is discussed in the section MYI Classification Algorithm.

## 2 Satellite data

The primary satellite data that were used in this study are the backscattering coefficient ( $\sigma_0$ ), the brightness temperature ( $T_b$ ) and the gamma-naught ( $\gamma_0$ ) in both the horizontal (HH) and vertical (VV) polarizations obtained from the ISRO's miniature satellite SCATSAT-1 (Fig. 1).

Indian Space Research Organisation's (ISRO) SCATSAT-1 (SC1) is a continuity mission to the bygone OceanSat-2. The satellite is at an altitude of 723 km above the earth's surface. It has a 1-m parabolic dish antenna and a dual feed assembly generate two Ku-band (operating at 13.515 GHz) conically scanning, pencil beams. The inner beam at an incidence angle of  $48.9^\circ$  has a swath of 1400 km with a scanning radius of 700 km. The outer beam with an incidence angle of  $57.6^\circ$  scans the ground with a swath of 1840 km at a scanning radius of 920 km. Moreover, the inner and outer beams are configured in horizontal (HH) and vertical (VV) polarization respectively for both transmit and receive modes. Revisit time is 2 days. The wind vector cell resolutions are either  $50 \times 50$  km or  $25 \times 25$  km. Assessment on the quality of SCATSAT winds vector have been carried out using in situ observations from tropical moored buoys or they found good quality of SCATSAT observations comparable with other similar observations<sup>12</sup>. Moreover, the observed normalized radar backscatter ( $\sigma_0$ ) over homogeneous natural calibration target like the Amazon rain-forest is stable within 0.5 dB among all observational variants such as ascending and descending passes (day and night) and fore and aft look directions<sup>13</sup>.

In this study, we used the super-resolution ( $0.225^\circ \times 0.225^\circ$ ) Level-4 Northern Hemisphere, 24-hr data archived at the Meteorological & Oceanographic Satellite Data Archival Centre (MOSDAC), Space Applications Centre-ISRO, Ahmedabad, India (<https://mosdac.gov.in/>). There data are generated using the Scatterometer Image Reconstruction technique from Level-1B data using both ascending and descending passes of  $\sigma_0$ ,  $\gamma_0$  and  $T_b$  for the past 24-hr<sup>14,15</sup>. More details on this dataset can be found in MOSDAC<sup>16</sup>.

The results obtained from the analysis are then compared with the sea ice type (SIT) data products archived at the EUMETSAT Ocean & Sea Ice Space Application Facilities- OSI SAF ([http://osisaf.met.no/p/ice/edge\\_type\\_long\\_description.html](http://osisaf.met.no/p/ice/edge_type_long_description.html)). At a grid resolution of 10 km and in polar stereographic projection, these daily data are generated using the brightness temperature data from SSMIS (19H, 19V,

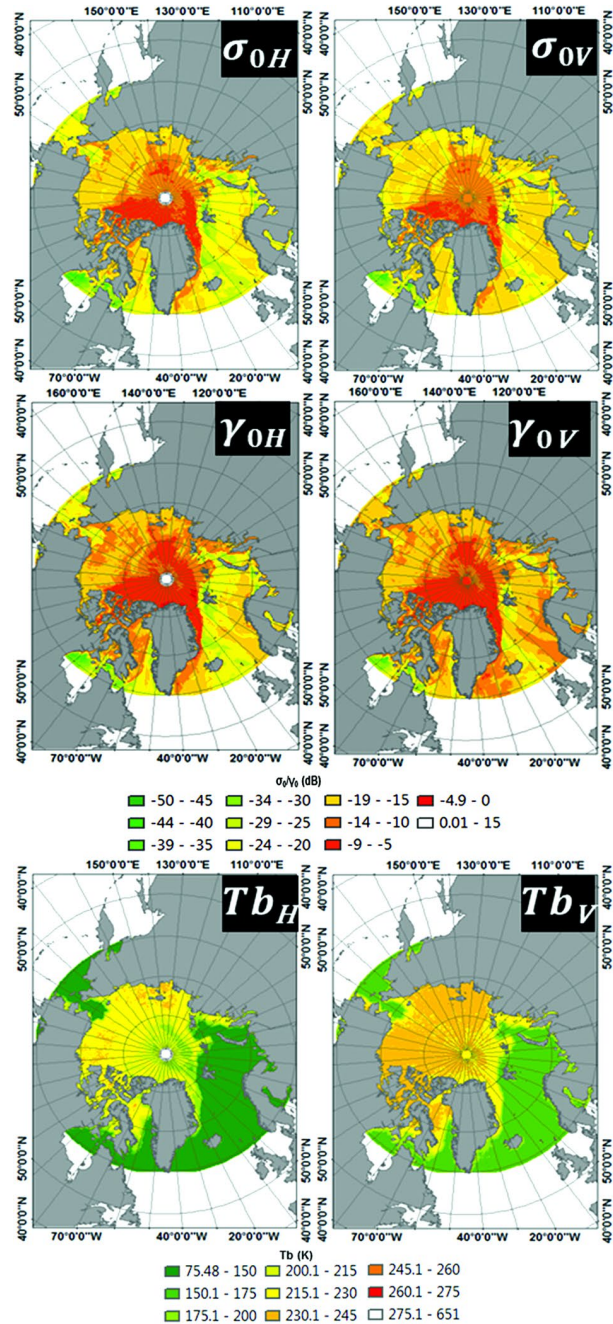


Fig. 1 — Super-resolution ( $0.225^\circ \times 0.225^\circ$ ) Arctic daily SCATSAT-1 variables- radar backscatter ( $\sigma_0$ ), gamma-naught ( $\gamma_0$ ) and the brightness temperature ( $T_b$ ).

37V, 91H, 91V which represent the frequency in GHz and the polarization) on board DMSP platform F18, AMSR-2 (19H, 19V, 37V, 89H, 89V) on board JAXA platform GCOM-W1, and backscatter data from ASCAT (C-band backscatter) on board EUMETSAT platform Metop-A and Metop-B. We also obtained sea ice edge (SIE) data products from OSI to generate shapefiles for the ice edge.

### 3 MYI classification algorithm

Before the classification algorithm is described, it may be worthy to discuss in brief some properties of MYI which will be useful in its distinction from the FYI. The microwave radiative characteristics of the Arctic MYI differ significantly those of FYI. This difference in characteristics has been exploited to monitor extent, variations, and dynamics of MYI in the Arctic using satellite data<sup>8</sup>.

Generally, MYI has higher albedo than FYI and, albedo is a function of thickness, surface temperature, and surface conditions<sup>17</sup>. Moreover, brine drainage from upper part of ice causes low salinity (resulting in different dielectric properties) in upper layer of MYI. This contributes to a difference in the dielectric properties of MYI compared to that of FYI. Therefore, the passive microwave signature of MYI is significantly different from that of FYI<sup>18,19</sup>.

At frequencies above 1 MHz, the dielectric constant ( $\epsilon'$ ) for sea ice is found to be relatively constant. However, the dielectric loss factor ( $\epsilon''$ ) differs. When  $\epsilon''$  is plotted versus frequencies, a minimum is obtained at 3–8 GHz, with higher values for lower and higher frequencies. Moreover, from empirical relationships it has also been found that the emissivity of seawater at 19 GHz and vertical incidence is about 0.44 compared with 0.92 for FYI and 0.84 for MYI. Because of the lower  $\epsilon''$  of MYI, microwave radiation penetrates deeper in MYI than it does so in FYI<sup>20</sup>. Characteristic of high and distinctive contrast between the MYI and FYI in the Ku-band backscatter fields have been used to delineate between them<sup>21</sup>.

In this study, we first apply the multivariate feature extraction technique of principal component analysis (PCA). The six SC1 variables namely,  $\sigma_0$ ,  $\gamma_0$  and  $T_b$  in both horizontal and vertical polarizations go as inputs to the PCA module in ENVI 4.5 (Forward PC Rotation). False-colour composite (FCC) formed by using the first three principal components (PC) explaining maximum variance of the data is shown in Fig. 2. The fluorescent greenish shade around the

central Arctic is the MYI, while the pink shaded region is the FYI. Clearly, the open ocean is segregated from the sea ice as seen as red and yellow in the figure. The black contour seen in the figure is the sea ice edge obtained from OSI SAF data. Thus, the technique discussed here can segregate sea ice from open ocean<sup>11</sup>. But in this study, we apply the sea ice boundary generated from the SIE data product archived at the OSI SAF to mask out regions outside the probable sea ice region for any given day.

The FCC generated above then goes to the classification module Iso Cluster Unsupervised Classification in ArcGIS which performs unsupervised classification on a series of input raster bands using ISODATA clustering and Maximum Likelihood techniques. More on these clustering techniques can be found elsewhere<sup>11,22</sup>. The classification result is shown in Fig. 3.

To study change detection, we perform the simple technique of image differencing provided in ENVI 4.5 module Change Detection Difference Map which produces an ENVI classification image characterizing the differences between any pair of initial state and final state images of the same scene at different times

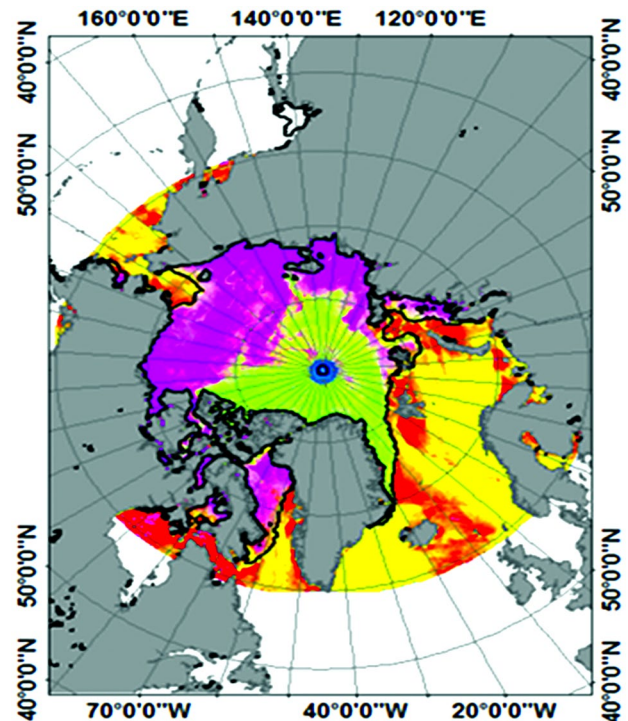


Fig. 2 — False-colour composite formed by using the first three principal components (PC) explaining maximum variance of the data. Black contour represents the Arctic sea ice extent for the day from EUMETSAT's Ocean & Sea Ice Space Application Facilities.

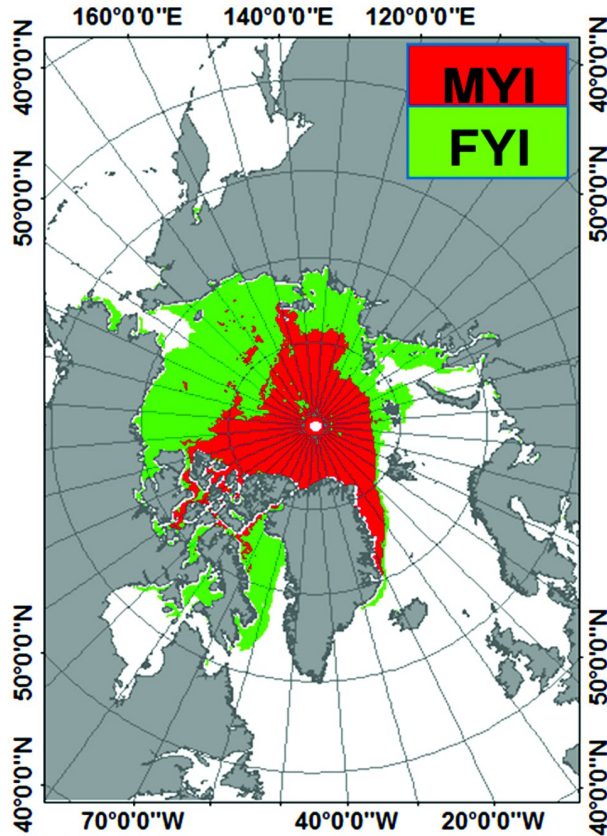


Fig. 3 — Classification of the Arctic multi-year ice (MYI) and first-year ice (FYI) using PCA+ISODATA classification on SCATSAT-1 data.

(subtracting an image of preceding year from the subsequent year). This procedure generates images for Autumn change (month of November) and the Spring change (March).

The entire work flow for the segregation of Arctic MYI from FYI and the change detection is given in Fig. 4.

The comparison results with the OSI SAF sea ice type and the change in the Arctic MYI are discussed in the next section.

#### 4 Quantitative analysis of MYI extents

SCATSAT-1 MYI extent is calculated by counting the number of MYI pixels observed in the data and multiplying by  $2.25 \times 2.25 \text{ km}^2$  (resolution of the data). Similarly, number of OSI SAF MYI pixels is multiplied by  $10 \times 10 \text{ km}^2$  (resolution of the data). Both extents are expressed in Mil km (million kilometre) for convenient.

In order to perform qualitative comparison, we have transformed the resolution of SCATSAT-1 data ( $2.25 \times 2.25 \text{ km}$ ) as similar to OSI SAF sea ice type data ( $10 \times 10 \text{ km}$ ). Numbers of common pixels, which

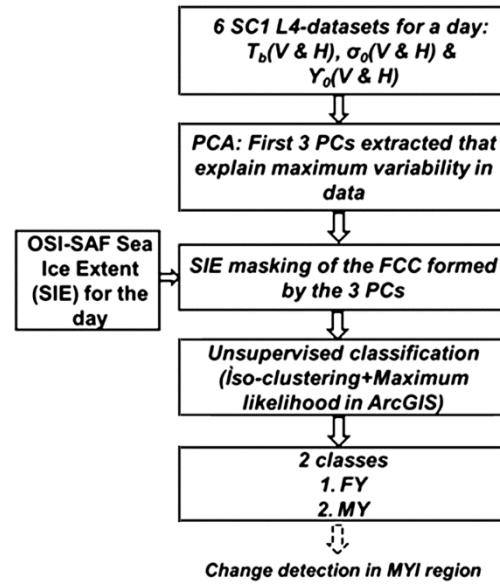


Fig. 4 — Work flow for the classification of Arctic MYI using SCATSAT-1 data.

show MYI characteristics, are counted by comparing extents of SCATSAT-1 MYI and OSI SAF MYI using the software ENVI-IDL. These numbers of common pixels are considered as correctly classified pixels (classified as MYI in SCATSAT-1 data). Therefore, the correct percentage of SCATSAT-1 MYI as compare to OSI SAF MYI is calculated as,

$$\text{Correct\%} = \frac{\text{Number of correctly classified pixels}}{\text{Number of MYI pixels in OSI data}} \times 100 \quad \dots (1)$$

#### 5 Results and Discussion

In order to carry out comparison analysis, we select the first day of each month from November, 2016 through March, 2018. However, there is no MYI classification in the OSI data from June, 2017 through September, 2017 as they all have been classified as ‘ambiguous’. Hence, there are thirteen data samples for comparison analysis.

Figure 5 shows one such instance of comparison. The red contour represents the sea ice boundary from the OSI SIE. Within this region, white region represents pixels with same classification of MYI in both SC1 & OSI; while the grey region denotes pixels classified as FYI in both SC1 and OSI. All other colours represent misclassifications (either MYI in SC1 and FYI in OSI or vice versa and tiny fractions of ocean misclassifications).

Per pixel comparison between SC1 derived MYI and MYI from OSI is carried out for the thirteen dates

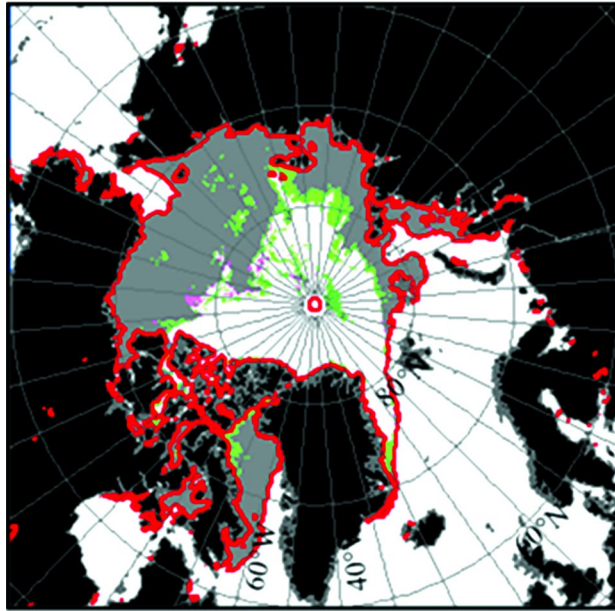


Fig. 5 — Comparison between SC1 derived MYI and the MYI obtained from OSI SAF sea ice type (SIT) for 1 December, 2016. Within the SIE (red contour- obtained from OSI), white region represents pixels with same classification of MYI in both SC1 & OSI SIT while grey region has both FYI pixels in both SC1 & OSI. All other colours represent misclassifications.

mentioned above (Fig. 6). In the figure, MY-MY represents classification of a pixel as MYI in both SC1 and OSI. Similarly, other classes are defined. OC represents open ocean.

We obtain an overall correct percentage of ~92% for both the MY-MY and FY-FY classes. The lowest correct classification for MY-MY class is a little over 62% on 1 March, 2017. An investigative study has been initiated to find the reason for this even though one probable reason could be the sudden change in radar backscatter signatures during transition period of spring/summer season due to snow surface melts.

Figure 7 gives the Arctic MYI extents in million km<sup>2</sup> for the period from November 2016 through March 2018 as obtained from the method discussed here (SC1) and the OSI. There is a RMS difference of 0.6 million km<sup>2</sup> between the two datasets. However, a statistical hypothesis test (two sample equal variance Student's t-test) has been carried out and it is found that at 95% confidence level, the variances in the two data samples (0.2541 in OSI and 0.255335 in SC1) do not differ statistically. Therefore, we do not reject the null hypothesis that at 95% confidence any difference between the two samples is due to chance and the sample means do not differ statistically<sup>23</sup>.

For change detection, we use the classified data of November 2016/2017 for autumn change and March

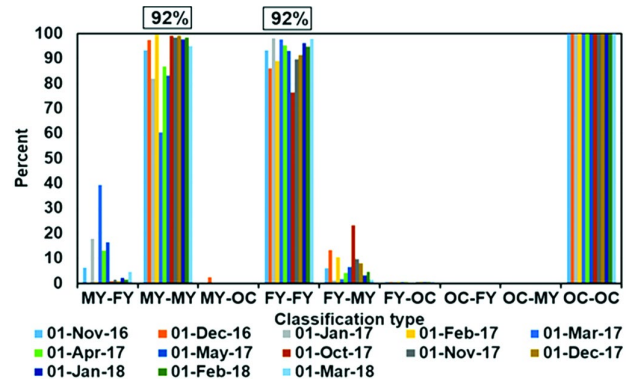


Fig. 6 — Percentage of correct/incorrect classification of SC1 derived MYI in comparison to the sea ice type from OSI SAF for thirteen individual days (first day of each month) from November, 2016 through March, 2018. There are data gaps from June through September, 2017.

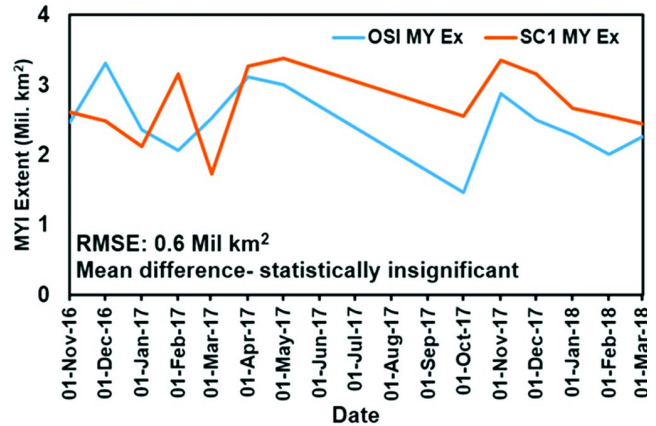


Fig. 7 — Arctic MYI extents (in million km<sup>2</sup>) from SC1 and OSI for the period November 2016 through March 2018.

2017/2018 for spring change. Autumn change is defined as the change associated with each pixel from a class to another class on 1 November of 2016 and 2017. Similar definition is used to define spring change on 1 March 2017 and 2018. To minimize ambiguities, we construct a shape file for either of the changes (autumn or spring) to define a sea ice boundary by taking a union of sea ice edges for the initial data and the final data. This is done using the Union function under Analysis Tools in ArcGIS which computes a geometric union of the input features.

Figure 8 shows the changes in the Arctic MYI for the study period. The colours represent the changes associated with each pixel except the blue colour which represents no change.

In autumn, there is a reduction in Arctic MYI (~0.656 million km<sup>2</sup>). Majority of this reduction

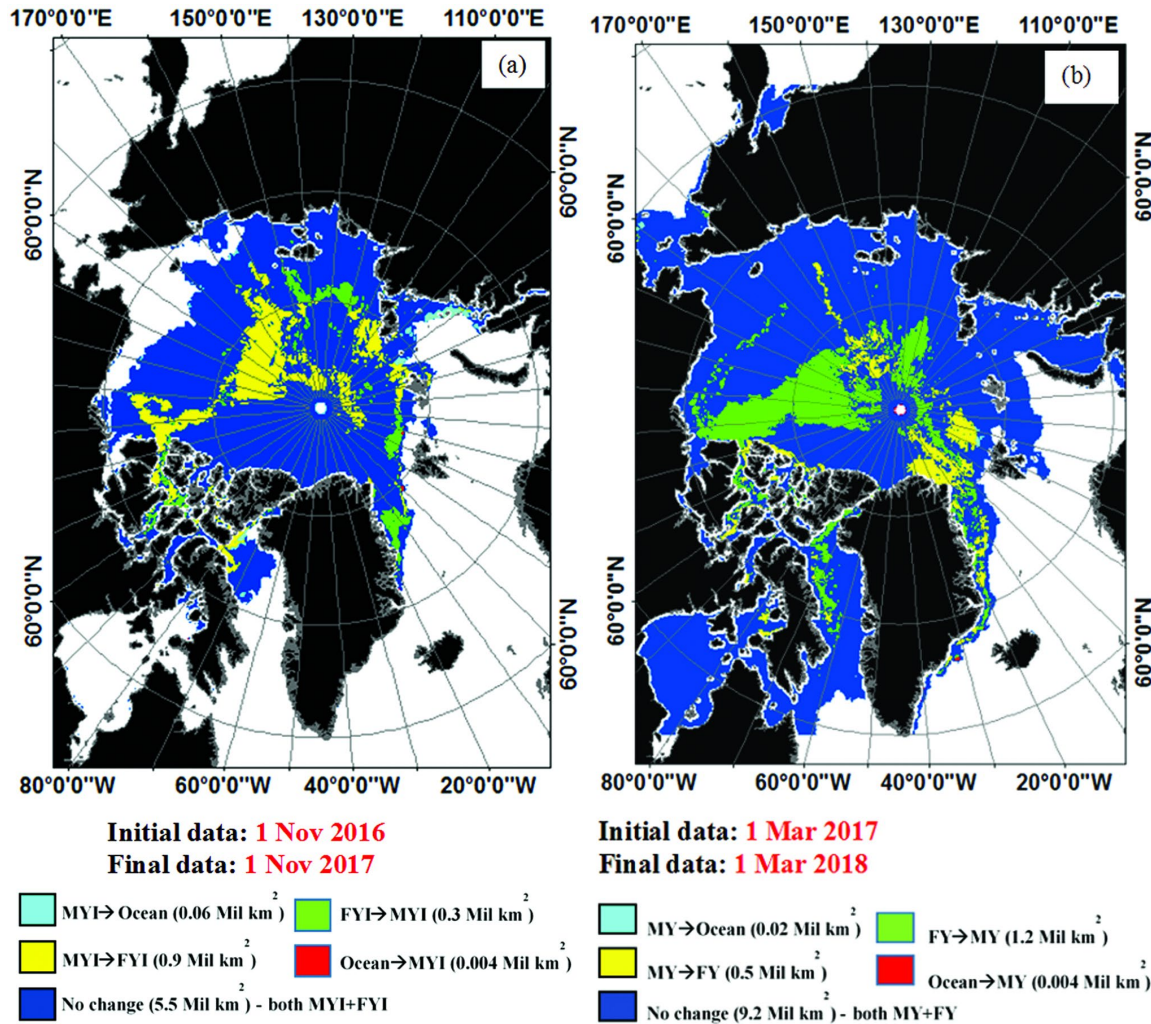


Fig. 8 — MYI change detection (a) for autumn (November 2016-2017) and (b) for spring (March 2017-2018). Sea ice boundaries for both the cases are taken as a union of the sea ice edges on the two dates considered for each season (e.g., 1 Nov. 2016 and 1 Nov. 2017 for autumn change and 1 Mar. 2017 and 1 Mar. 2018 for spring change). These boundaries are then overlaid as shape files on the images to mask out the ocean and land surfaces. The coloured rectangular boxes on the right of each figure denote the change associated with each pixel. Blue represents no change. Extent change in million km<sup>2</sup> is given within brackets.

occurs in places like the Central Arctic, the Beaufort Sea and the Laptev Sea. However, the spring change is marked by an increase in MYI by about 0.684 million km<sup>2</sup> with the major increase taking place at the Beaufort Sea and the Central Arctic. There are patches of areas in East Greenland Sea where reduction in MYI (changing to FYI) can be observed.

### 6 Conclusions

In this paper, an attempt has been made to segregate multi-year ice from first-year ice in the Arctic. It is a generally understanding that multi-year ice tends to survive longer in the Arctic than that in the Antarctic due to geographical differences between the two hemispheres.

Super-high resolution (~0.225°) satellite data from ISRO’s SCATSAT-1 have been used to achieve the goal of segregation by employing the techniques of feature extraction and cluster classification.

When compared with popular sea ice type product from EUMETSAT OSI SAF, very good results were obtained which increases our confidence that the method can be employed for sea ice type’s discrimination.

Preliminary change detection is also carried out to ascertain changes in the multi-year fraction of the Arctic sea ice.

### Acknowledgement

The authors would like to thank an anonymous reviewer for reviewing the manuscript. All the data

archival repositories are duly acknowledged for the datasets used in this study.

## References

- 1 Ye Y, Heygster G & Shokr M, *IEEE Transactions on Geoscience and Remote Sensing*, 54 (2016) 2602.
- 2 Scott M & Hansen K, <https://earthobservatory.nasa.gov/features/SeaIce>, (2016).
- 3 <https://nsidc.org/cryosphere/seaice/characteristics/multiyear.html> (12 December, 2018).
- 4 Swan A M & Long D G, *IEEE Transactions on Geoscience and Remote Sensing*, 50 (2012) 3317.
- 5 Comiso J C, *Journal of Climate*, 25 (2012) 1176.
- 6 Kwok R, Cunningham G, Wensnahan M, Rigor I, Zwally H & Yi D, *Journal of Geophysical Research*, 114 (2009) C07005.
- 7 Kwok R, *Environmental Research Letters*, 13 (2018) 105005.
- 8 Comiso J, *Journal of Geophysical Research*, 95 (1990) 13411.
- 9 Lindell D B & Long D G, *MDPI Remote Sensing*, 8 (2016) 688.
- 10 Ezraty R & Cavanié A, *Journal Geophysical Research*, 104 (1999) 11471.
- 11 Singh U S & Singh R K K, *Remote Sensing Applications: Society and Environment*, 18 (2020) 100310.
- 12 Johny C J, Singh S K & Prasad V S, *Pure and Appl. Geophysics*, 176 (2019) 2659.
- 13 <https://directory.eoportal.org/web/eoportal/satellite-missions/s/scatsat-1>, (1 January, 2020).
- 14 Long D, Hardin P & Whiting P, *IEEE Transactions on Geoscience and Remote Sensing*, 31 (1993) 700.
- 15 Early D & Long D, *IEEE Transactions on Geoscience and Remote Sensing*, 39 (2001) 291.
- 16 *SCATSAT-1 Level 4 Data Products Format Document, SCATSAT-1 Level 4 Data Products Format Document Ver. 1.1* (Space Applications Centre-ISRO, Ahmedabad), 2017.
- 17 Hwang B J, Ehn J K & Barber D G, *Geophysical Research Letters*, 33 (2006) L17503.
- 18 Vant M R, Ramseier R O & Makios V, *Journal of Applied Physics*, 49 (1978) 1234.
- 19 Comiso J C, *Journal of Climatology*, 25 (2011) 1176.
- 20 Sandven S, Johannessen O M & Kloster K, in *Encyclopedia of Analytical Chemistry*, edited by Meyers R A (John Wiley & Sons, Ltd) (2006) A2320.
- 21 Kwok R, *Journal of Geophysical Research*, 109 (2004) C11.
- 22 Lillesand T M, Kiefer R W and Chipman J W, *Remote Sensing and Image Interpretation*, 6<sup>th</sup> edn, (John Wiley & Sons, New York), (2011) 756.
- 23 <https://www.itl.nist.gov/div898/handbook/eda/section3/eda353.html> (2020).